

Effect of Annealing Time on the Dielectric Properties of BaMn₃Ti₄O_{14.25} Pellets by Spark Plasma Sintering

Xiong Xie^{1,2}, Jun Shen^{1*}, Xinxin Liu², Liang Wang²

¹State Key Laboratory of Mechanical Transmission, College of Materials science and engineering, Chongqing University, Chongqing, China

²Chongqing Institute of Green and Intelligent Technology, Chinese Academy of Sciences, Chongqing, China

Email: xiexiong@cqu.edu.cn, *shenjun@cqu.edu.cn, liuxinxin@cigit.ac.cn, wangliang@cigit.ac.cn

How to cite this paper: Xie, X., Shen, J., Liu, X.X. and Wang, L. (2019) Effect of Annealing Time on the Dielectric Properties of BaMn₃Ti₄O_{14.25} Pellets by Spark Plasma Sintering. *Journal of Applied Mathematics and Physics*, 7, 1637-1644.

<https://doi.org/10.4236/jamp.2019.78111>

Received: July 22, 2019

Accepted: August 9, 2019

Published: August 12, 2019

Abstract

In this paper, the effects of annealing time on the dielectric properties of the Spark Plasma Sintered (SPS) BaMn₃Ti₄O_{14.25} pellets were detail studied by the crystal structure analysis, micro structural observation and electrical properties research. The results showed that long annealing time was beneficial to the recovery of crystal structure damage caused by SPS, the formation of a reoxidation layer at the surface of grains and decreasing of the electrically insulating phase. All of these resulted in an increase in dielectric constant and loss, and a reduction in breakdown voltage.

Keywords

BaMn₃Ti₄O_{14.25}, Dielectric Properties, Reoxidation Layer, Electrically Insulating Phase Breakdown Voltage

1. Introduction

Transition metal based oxides have been a longstanding research focus due to their distinguish properties and wide range applications [1] [2] [3]. Recently, the discovery of new complex oxides, BaMn₃Ti₄O_{14.25}, named BMT, exhibited ferroelectricity, an antiferromagnetic phase transition ($T_N \sim 120$ K) with a weak ferromagnetic ordering at lower temperatures ($T_F \sim 42$ K). In addition, they also showed a giant dielectric constant at low frequency ($>10^4$ at 1 kHz) and a stable intrinsic high dielectric constant (~ 1000 at 1 MHz). It is an excellent performance indicator for dielectric materials due to most researched materials cannot keep their giant/high dielectric constant at high frequency. Such as, the popular

non-ferroelectric giant dielectric constant perovskite oxide, $\text{CaCu}_3\text{Ti}_4\text{O}_{12}$ (CCTO), only can hold its high dielectric constant at lower frequency, but the dielectric constant reduced sharply with increased frequency and even to lower than 100 when the frequency is over megahertz [4]. The giant dielectric constant ferroelectric perovskite oxide, BaTiO_3 (BTO), could only maintain the giant dielectric constant ($>10^4$) at a very narrow temperature range and resulted the transition of paraelectric to ferroelectric when the temperature over the phase temperature (T_m). Moreover, the poling polycrystalline counterparts are about thousands, which would significantly reduce when the applied frequency is over megahertz [5] [6] [7].

Such outstanding dielectric performance for BMT were derived from the existence of significant electron correlations which result in charge order, and/or Ti^{4+} based dipolar distortion, below the critical field strength for ferroelectricity. The large intrinsic dielectric constant mainly contributed by the internal barrier layer capacitance (IBLC). In the crystal structure of BMT, the chains of edge-shared TiO_6 octahedra act as barrier layers which similar to the case reported for $\text{CaCu}_3\text{Ti}_4\text{O}_{12}$ (CCTO) [8]. Compare with the CCTO, the existence of mixed-valence Mn ions in BMT. The valence of manganese ions alternates between +3 and +4 at room-temperature to construct a so-called charge disordered system, which maybe the main reason for that BMT can hold their high dielectric constant in high frequency range.

However, the giant dielectric effect of BMT lacks systematic research, although some reports have been published in previous studies [9] [10]. In this paper, by changing the annealing time of the spark plasma sintering (SPS) BMT pellets and combining the microstructure analysis, impedance test and current-voltage test, the giant dielectric effect and breakdown voltage of BMT were systematically studied.

2. Experimental Details

The as-fabricated BMT nanocrystals, prepared by our developed gel self-collection [9], were used as raw materials to prepare SPS pellets. A SPS apparatus (Dr. Sinter, SPS 625, Fuji Electronic Industrial Co. Ltd. Japan) was used to sinter BMT powder into BMT pellets. A certain amount of as-calcined nanocrystals were putted into the graphite mold with the diameter of 10 mm, and then sintered at the temperature of 720°C for 5 minutes in vacuum of 8 MPa with a pressure of 42 MPa. To remove carbon from the sample, these samples were annealed in an 800°C muffle furnace for 4 and 24 hours, respectively. For the sake of distinction, we named the samples obtained under the two processes as SPS-BMT-4 h and SPS-BMT-24 h. The crystal structure was characterized by X-ray power diffraction (XRD). A scanning electron microscopy (FE-SEM, JSM-7800F) was used to measure the grain size of nanoparticles and observe morphology of polished SPS samples. For electrical characterization, the pellet surfaces were first thoroughly polished and then covered on both sides with silver paste. Frequency

dependent dielectric properties and impedance performance of pellets were measured by Aglient E4980A LCR meter. Electrical properties were carried out by Keithley 4200 semiconductor measurement comprehensive analyzer.

3. Results and Discussion

The crystal structure and SEM morphologies of sample of BMT, SPS-BMT-4 h and SPS-BMT-24 h are shown in **Figure 1**. As we previous discussed, the BMT belongs to hollandite group (Redledgeite structure, space group 87, $I/4m$), $A^{II}[M^{IV}, M^{III}]_8O_{16}$, the Mn and Tications are located inside corner- and edge-shared oxygen octahedral with Ba cations in the channels. In this instance the fractional oxygen of the unit cell balances the $Mn^{+3}: Mn^{+4}$ 1:1 ratio. The detail crystal structure of the BMT was presented in our previous paper [9]. As seen in **Figure 1(a)**, although some XRD diffraction pattern of SPS-BMT-4 h have low intensity and even they cannot be clearly identified, the XRD patterns of SPS-BMT-4 h and SPS-BMT-24 h were in accordance with those of BMT, which proves that the BMT pellets after SPS and annealing could maintain the original crystal structure. As shown in **Figure 1(b)** and **Figure 1(c)**, compared with those of SPS-BMT-24 h, some agglomerates appear in the sample of

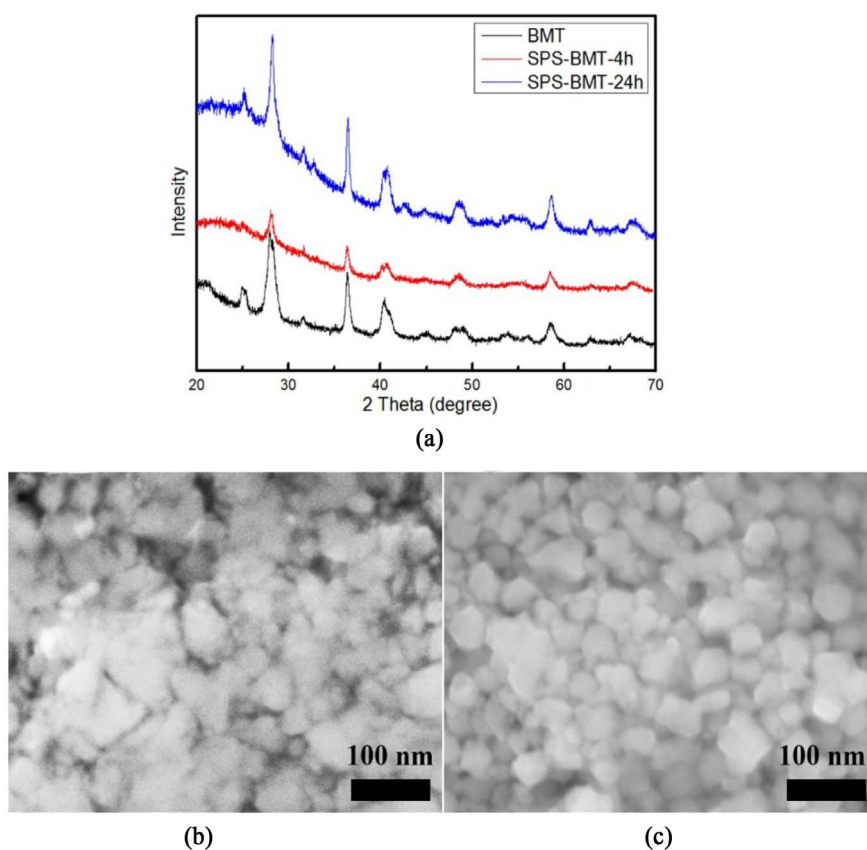


Figure 1. (a) The XRD patterns of BMT (black line), SPS-BMT-4 h (red line) and SPS-BMT-24 h (blue line). (b) and (c) SEM morphologies of SPS-BMT-4 h, SPS-BMT-24 h, respectively.

SPS-BMT-4 h and the grain boundary is inconspicuous. During SPS process, the grain surface may form an amorphous phase due to local or transient high temperature, and impurities such as oxides on the surface of the raw material powder may also aggravate the amorphous phase [11]. In the subsequent annealing and carbon removal process, BMT crystal recrystallize and grow again at 800 °C, which is beneficial to the crystallization and growth of crystal grains and then eliminate the amorphous phase for BMT. Moreover, the longer the annealing time, the more obvious the crystal structure recovery. Therefore, the amorphous phase and reduced XRD patterns appeared in the sample of SPS-BMT-4 h due to SPS and inadequate recovery of crystal structure. When the annealing time prolong to 24 h, the amorphous phase completely abolished and crystal structure of BMT fully recovered.

Figure 2(a) and Figure 2(b) show the impedance complex plane plot, Z^* , for SPS BMT pellets annealing for 4 and 24 h. As we can see, the impedance spectroscopy (IS) present a semi-circular with non-zero intercept on the Z' axis at high frequencies. Both of the impedance data can be ideally described by parallel resistor-capacitor circuit (resistor, R and capacitor, C) elements, as seen

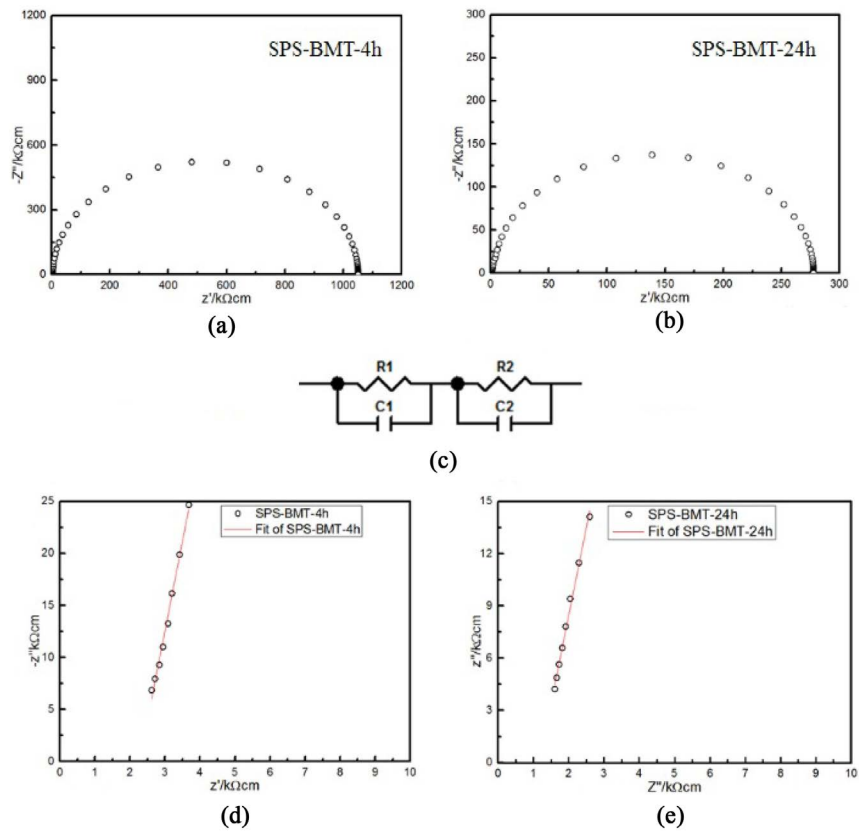


Figure 2. Impedance complex plane plot, Z^* at ~300 K for sample of (a) SPS-BMT-4h and (b) SPS-BMT-24 h. (c) shows the appropriate equivalent electric circuits; (d) and (e) show an expanded view of complex impedance (solid black squares) and fitting plots (solid red line) of the high frequency data close to the origin for SPS-BMT-4h and SPS-BMT-24 h, respectively.

in **Figure 2(c)**. One RC element refers to the semiconducting grains. Based on the linear fit results, the resistivity of semiconducting grains is $\sim 2.27 \text{ K}\Omega\cdot\text{cm}$ and $1.09 \text{ K}\Omega\cdot\text{cm}$ for the sample of SPS-BMT-4 h and SPS-BMT-24 h, respectively. The other RC element refers to the “leaky” grain boundary (GB) regions, which give rise to the large arc of $\sim 1.05 \text{ M}\Omega\cdot\text{cm}$ and $0.29 \text{ M}\Omega\cdot\text{cm}$ for pellets annealed at 4 and 24 h, respectively. The semiconducting grains maybe oxygen stoichiometric and exhibit intrinsic semiconductivity, which also be found in the $\text{Ca-Cu}_3\text{Mn}_4\text{O}_{12}$ [12]. Based on the oxygen-stoichiometric model, an electrically insulating secondary phase existed at the grain boundaries.

Figure 3 shows the frequency dependent dielectric constants and losses of sample of SPS-BMT-4 h and SPS-BMT-24 h. It is apparent that the dielectric constant and loss of sample of SPS-BMT-24 h is much higher than those of the sample of SPS-BMT-4 h in all tested frequencies ranges. The dielectric constant decreased sharply with the increased frequency at low frequency range. After about 20 kHz, one distinct permittivity plateaus are shown at high frequency. The variation law of loss with increased frequency was showed in **Figure 2(b)**, which present a minimum value of about 0.23 and 0.35 at 100 kHz for the sample of SPS-BMT-4 h and SPS-BMT-24 h, respectively. In the frame work of dielectric relaxations represented by RC elements, the high-permittivity at low frequencies range primarily originated from the GB contribution, while the low permittivity plateau at high frequencies primarily originates from the bulk contribution. As the annealing time increased, the dielectric constant of the SPS sample increases dramatically. This interesting feature is related to the differences in ceramic microstructure. As previous reported [8] [13], the “giant” permittivity value for long-time sintered CCTO sample is associated with the presence of a thin reoxidized grain boundary regions on the outer surfaces of the large semiconducting grains or to a electrically insulating secondary phase at the grain boundaries. The reoxidation layer of grain outer would produced Schottky barriers and associated space charge regions that penetrate only the outer regions of the semiconducting grains and which result in giant dielectric constant for the long time annealing sample of SPS-BMT-24 h. The electrically insulating secondary phase may decrease with the increase of annealing time.

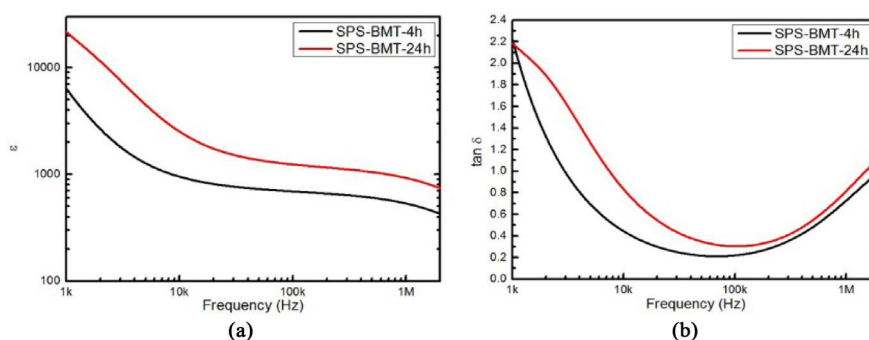


Figure 3. Frequency dependent dielectric constants (a) and losses (b) of sample of SPS-BMT-4 h and SPS-BMT-24 h.

And then the semiconductivity would increase to result in an increase of permittivity. Both models would give rise to high and frequency independent ϵ value. A disadvantage of long time annealing for SPS BMT sample is their higher loss and lower threshold to breakdown voltage. So, as seen in **Figure 3(b)**, the dielectric loss of sample of SPS-BMT-4 h is lower than that of SPS-BMT-24 h.

Moreover, Measurements of I-V characteristics were made on SPS-BMT-4 h and SPS-BMT-24 h pellets. **Figure 4** shows plots of current density (J) against electric field (E) for polycrystalline specimens annealed at 4 and 24 h, respectively. As shown in the **Figure 4(a)** and **Figure 4(b)**, a strongly nonlinear relationship is observed, clearly marking the breakdown voltage varies considerably with the annealing time pellets: 1700 V/cm for the sample of SPS-BMT-4 h and 1000 V/cm for the SPS-BMT-24 h, respectively. This decreased breakdown voltage with increased annealing time maybe induced by the semiconductivity in the grains. The grains may be oxygen stoichiometric and intrinsic semiconductivity, as occurred in the structurally related $\text{CaCu}_3\text{Mn}_4\text{O}_{12}$ [12]. Moreover, the decreased electrically insulating secondary phase also increased the intrinsic semiconductivity of BMT ceramics. Therefore, with increased annealing time, the breakdown voltage of the BMT ceramics decreased. In addition, **Figure 4(c)** and **Figure 4(d)** represents the frequency dependent dielectric property of the sample of SPS-BMT-4 h and SPS-BMT-24 h after 1 hour of I-V Measurements. This test result indicates that the dielectric properties of $\text{BaMn}_3\text{T}_{14}\text{O}_{14.25}$ are recoverable when the high voltages are removed.

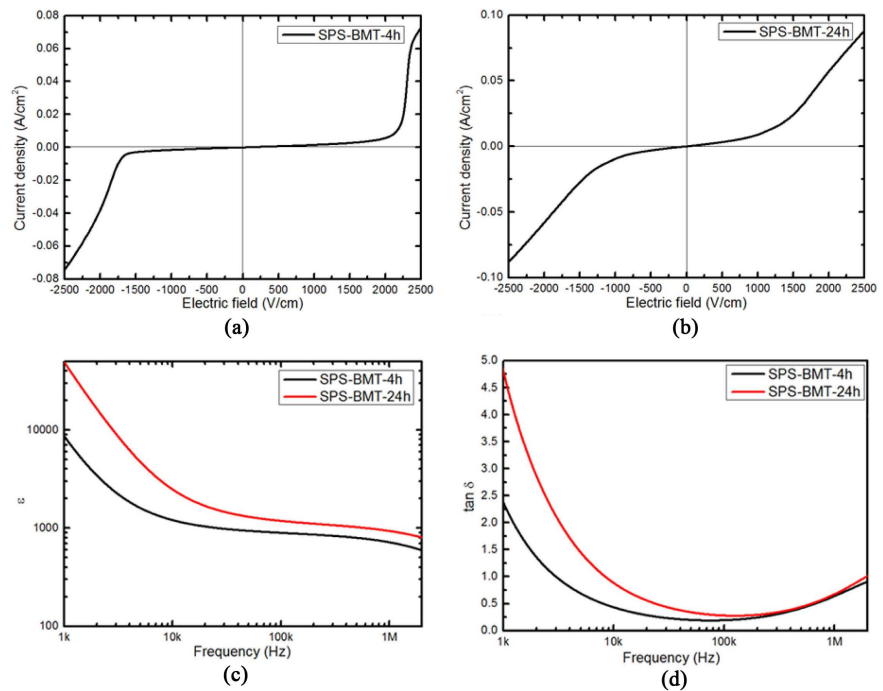


Figure 4. Current density-electric field (J-E) characteristics of samples of (a) SPS-BMT-4 h (b) SPS-BMT-24 h. The log-log plot (c) and (d) shows the frequency dependent dielectric property of the sample of SPS-BMT-4 h and SPS-BMT-24 h after breakdown 1 hour.

4. Conclusion

By extending the annealing time from 4 h to 24 h at 800°C, the crystal structure is effectively restored and the reoxidation layer on the surface of grains is formed. Based on these phenomena, the dielectric constant increased from ~6000 to ~20,000 at 1 kHz, However, both of the decreased the electrically insulating secondary phase with the increased annealing time and the Schottky barriers and associated space charge regions produced by the reoxidation layer of grain outer would enhance the semiconductivity of the BMT pellets, resulting in the dielectric loss increased from 0.23 to 0.35 at 100 kHz, while the breakdown voltage decreased from 1700 V/cm to 1000 V/cm. Moreover, the dielectric properties of $\text{BaMn}_3\text{T}_{14}\text{O}_{14.25}$ can be recoverable after the high voltages are removed.

Conflicts of Interest

The authors declare no conflicts of interest regarding the publication of this paper.

References

- [1] Huang, L.M., Jia, Z., Kymissis, I. and O'Brien, S. (2010) High K Capacitors and OFET Gate Dielectrics from Self-Assembled BaTiO_3 and $(\text{Ba,Sr})\text{TiO}_3$ Nanocrystals in the Superparaelectric Limit. *Adv. Funct. Mater.*, **20**, 554-560. <https://doi.org/10.1002/adfm.200901258>
- [2] Namiki, Y., Namiki, T., Yoshida, H., Ishii, Y., Tsubota, A., Koido, S., Nariai, K., Mitsunaga, M., Yanagisawa, S., Kashiwagi, H., Mabashi, Y., Yumoto, Y., Hoshina, S., Fujise, K. and Tada, N. (2009) A Novel Magnetic Crystal-Lipid Nanostructure for Magnetically Guided *in Vivo* Gene Delivery. *Nat. Nanotechnol.*, **4**, 598-606. <https://doi.org/10.1038/nnano.2009.202>
- [3] Liang, Y.Y., Li, Y.G., Wang, H.L., Zhou, J.G., Wang, J., Regier, T. and Dai, H.J. (2011) Co_3O_4 Nanocrystals on Graphene as a Synergistic Catalyst for Oxygen Reduction Reaction. *Nat. Mater.*, **10**, 780-786. <https://doi.org/10.1038/nmat3087>
- [4] Homes, C.C., Vogt, T., Shapiro, S.M., Wakimoto, S. and Ramirez, A.P. (2001) Optical Response of High-Dielectric-Constant Perovskite-Related Oxide. *Science*, **293**, 673-676. <https://doi.org/10.1126/science.1061655>
- [5] Zgonik, M., Bernasconi, P., Duelli, M., Schlessler, R., Garrett, M.H., Rytz, D., Zhu, Y. and Xu, X. (1994) Dielectric, Elastic, Piezoelectric, Electro-Optic, and Elasto-Optic Tensors of Crystals. *Phys. Rev. B*, **50**, 5941-5949. <https://doi.org/10.1103/PhysRevB.50.5941>
- [6] Zheng, P., Zhang, J.L., Tan, Y.Q. and Wang, C.L. (2012) Grain-Size Effects on Dielectric and Piezoelectric Properties of Poled BaTiO_3 Ceramics. *Acta Mater.*, **60**, 5022-5030. <https://doi.org/10.1016/j.actamat.2012.06.015>
- [7] Han, H., Voisin, C., Guillemet-Fritsch, S., Dufour, P., Fenailleau, C., Turner, C. and Nino, J.C. (2013) Origin of Colossal Permittivity in BaTiO_3 via Broadband Dielectric Spectroscopy. *J. Appl. Phys.*, **113**, Article ID: 024102. <https://doi.org/10.1063/1.4774099>
- [8] Adams, T.B., Sinclair, D.C. and West, A.R. (2002) Giant Barrier Layer Capacitance Effects in $\text{CaCu}_3\text{Ti}_4\text{O}_{12}$ Ceramics. *Adv. Mater.*, **14**, 1321-1323. [https://doi.org/10.1002/1521-4095\(20020916\)14:18<1321::AID-ADMA1321>3.0.CO;2-P](https://doi.org/10.1002/1521-4095(20020916)14:18<1321::AID-ADMA1321>3.0.CO;2-P)

- [9] Liu, S., Akbashev, A.R., Yang, X., Liu, X., Li, W., Zhao, L., Li, X., Couzis, A., Han, M.-G., Zhu, Y., Krusin-Elbaum, L., Li, J., Huang, L., Billinge, S.J.L., Spanier, J.E. and O'Brien, S. (n.d.) Hollandites as a New Class of Multiferroics. *Sci. Rep-UK*.
- [10] Liu, S., Li, W., Li, J. and O'Brien, S. (2015) Electrical Properties of New Hollandite-Complex Oxide Nanocrystals. *J. Nanosci. Nanotechnol*, **15**, 7074-7080. <https://doi.org/10.1166/jnn.2015.10545>
- [11] Wang, L., Chen, D., Zhang, H. and Tong, J. (2009) Structure and Mechanical Properties of Densified Boron Carbide Ceramics by SPS. *Rare Metal Mat. Eng.*, **38**, 529-532.
- [12] Weht, R. and Pickett, W.E. (2001) Magnetoelectronic Properties of a Ferrimagnetic Semiconductor: The Hybrid Cupromanganite $\text{CaCu}_3\text{Mn}_4\text{O}_{12}$. *Phys. Rev. B*, **65**, Article ID: 0144151. <https://doi.org/10.1103/PhysRevB.65.014415>
- [13] Schmidt, R., Stennett, M.C., Hyatt, N.C., Pokorny, J., Prado-Gonjal, J., Li, M. and Sinclair, D.C. (2012) Effects of Sintering Temperature on the Internal Barrier Layer Capacitor (IBLC) Structure in $\text{CaCu}_3\text{Ti}_4\text{O}_{12}$ (CCTO) Ceramics. *J. Eur. Ceram. Soc.*, **32**, 3313-3323. <https://doi.org/10.1016/j.jeurceramsoc.2012.03.040>